PHOTONICS Research

# Enhancing plasmonic trapping with a perfect radially polarized beam

Xianyou Wang,[1,†] Yuquan Zhang,[1,†] Yanmeng Dai,[1] Changjun Min,[1,2] and Xiaocong Yuan[1,3]

[1]Nanophotonics Research Center, Shenzhen Key Laboratory of Micro-Scale Optical Information Technology, Shenzhen University, Shenzhen 518060, China
[2]e-mail: cjmin@szu.edu.cn
[3]e-mail: xcyuan@szu.edu.cn

Received 17 April 2018; revised 27 June 2018; accepted 4 July 2018; posted 6 July 2018 (Doc. ID 328577); published 8 August 2018

**Strong plasmonic focal spots, excited by radially polarized light on a smooth thin metallic film, have been widely applied to trap various micro- and nano-sized objects. However, the direct transmission part of the incident light leads to the scattering force exerted on trapped particles, which seriously affects the stability of the plasmonic trap. Here we employ a novel perfect radially polarized beam to solve this problem. Both theoretical and experimental results verify that such a beam could strongly suppress the directly transmitted light to reduce the piconewton scattering force, and an enhanced plasmonic trapping stiffness that is 2.6 times higher is achieved in experiments. The present work opens up new opportunities for a variety of research requiring the stable manipulations of particles.** 

***OCIS codes:*** (260.5430) Polarization; (350.4855) Optical tweezers or optical manipulation; (250.5403) Plasmonics.

https://doi.org/10.1364/PRJ.6.000847

## 1. INTRODUCTION

Optical traps, originating from forces induced by electromagnetic fields, have been extensively used as a powerful scientific tool to study the physical, chemical, and biological characteristics of micro-/nano-objects [1,2]. Metal particles, based on their special chemical and physical properties, possess extensive applications in various areas including spectroscopy, catalysis, and bio-/medical science and techniques [3]. However, it is well known that metallic particles are hard to trap by traditional optical tweezers due to their high absorption and reflection features. Recently, many approaches have been proposed to enhance the gradient force or suppress the scattering force to increase the trapping efficiency, such as trapping of Rayleigh particles [4,5] or employing plasmonic nanostructures [6–8]. However, high precision and strong robustness and dynamics are hard to achieve at the same time. Focused plasmonic tweezers, which are based on surface plasmon polarizations (SPPs) excited on a thin metal film, have exhibited an enhanced attractive force for trapping various micro- and nano-sized metallic particles and nanowires [9–11]. Such a trapping technique has shown great potential in many applications, such as the fabrication of nanostructures [12,13], detection of orbital angular momentum (OAM) [14,15], and dynamic surface-enhanced Raman spectroscopy (SERS) for single molecule detection [11,16,17].

To achieve high performance of the plasmonic tweezers in such applications, the trapping stiffness is a key issue. Stable trapping and manipulation of particles are in high demand in nanofabrication, sensing, and quantum technologies, which actively promotes the development of techniques for trapping stiffness improvement. However, plasmonic trapping stiffness is inevitably affected in various terms from the Brownian movement to thermal convection [18]. The most direct way to enhance the stiffness is by reducing the negative heating effect; thus, cooling has become a popular method and has been widely used in trapping systems [19,20]. Nevertheless, the cooling module is always cumbersome, and in the all-optically excited SPP trapping systems, the thermal effect is not strong [9], resulting in a limited improvement in trapping stiffness. Besides cooling, another candidate for stiffness enhancement is by enhancing the trapping gradient force and suppressing the repulsive scattering force, which requires refined designs of the excited plasmonic fields as well as the incident light beams.

In this work, we investigate how to reduce the scattering force and enhance the plasmonic trapping stiffness through a novel perfect radially polarized beam (PRPB) [21]. Although the radially polarized beam (RPB) is an effective way to excite the focused SPP field for trapping [9], its directly transmitted light through the thin metallic film causes a strong scattering force acting on the particle to strengthen the Brownian movement. Here, based on theoretical and experimental studies, we demonstrate an effective method for improving plasmonic trapping stiffness by employing two axicons to compress the incident RPB into a PRPB. The whole energy of the generated

PRPB is confined into a very sharp ring with tunable diameter to fit the SPP exciting angle. Consequently, most direct transmission through the metallic film is suppressed, while the exciting efficiency of SPP is increased to provide a stronger trapping force. The experimental results verify the enhancement of the trapping stiffness and present the reduced Brownian movement. We believe that this method could become a very practical way for enhancing the performance of plasmonic trapping and manipulation in chemical and physical lab-on-a-chip research.

## 2. EXPERIMENTAL SETUP AND METHODS

In the all-optically excited SPP tweezers [4], RPB is usually employed due to its high SPP coupling efficiency compared with other polarizations [22]. However, when the RPB is tightly focused onto the metal film by a high-numerical-aperture (NA) objective, the SPP is only excited at the strict angle that satisfies the wavevector matching condition. The light of the RPB at other angles is reflected, absorbed, or transmitted by the metal film, where the transmitted part would increase the scattering force and the absorbed part would generate heat, both decreasing the trapping stiffness. To reduce the influences of the transmitted and absorbed lights, there is a simple choice to block the inner transmitted part of the RPB [23]; however, most of the energy is wasted and the SPP exciting efficiency is not improved. To further enhance the SPP exciting efficiency, the best choice is to concentrate the whole energy of the light into a very sharp ring to fit the SPP exciting angle.

The recently developed perfect optical vortices (POVs) provide a good candidate that can confine all incident energy into a sharp bright ring with a tunable radius independent on the topological charge [24–26]. Here, the idea of PRPB follows the concept of a POV beam whose topological charge is set to be zero and whose polarization state is chosen as radial polarization. The PRPB can be efficiently generated by two coaxial axicons in an experiment with a tunable radius [27,28].

Herein, a PRPB-based plasmonic tweezers configuration is proposed that employs two axicons to compress the incident RPB into a thin PRPB for establishing a stiffness enhanced trap, as shown in Fig. 1(a). The incident beam is first expanded by using a telescope system (L1 and L2). Then it becomes linearly polarized by a polarizer (P1), and the polarization is modulated by a half-wave plate (HWP). A vortex retarder (VR, Thorlabs Inc.) is employed to generate the RPB, and another telescope system (L3 and L4) is used to expand the beam to fit the back aperture of the highly focused objective (NA = 1.49). A PRPB could be generated from a RPB by replacing the telescope system (L3, L4) with two coaxial axicons (A1, A2). Then the energy could be confined into a thin ring, and the parallel annular beam diameter can be modulated by changing the distance between A1 and A2 [26].

The generated RPB or PRPB is then tightly focused by an objective (NA = 1.49) onto the bottom of a gold film. The gold film with a thickness of 50 nm was coated onto a cleaned glass coverslip using thermal evaporation deposition to excite the plasmonic trapping field. The gap between the objective lens and the glass substrate is filled with index-matching oil. Gold particles (0.5–1.0 μm, Alfa Aesar Inc.) were diffused into water and dripped onto the gold film as trapping samples. From CCD2, the trapping process under a self-built dark field illumination (light-emitting diode, LED) could be captured in time.

Figure 1(b) depicts the SPP excitation process by a focused RPB. When the RPB is focused onto the bottom of the gold film, a small part of the RPB (whose deflection angle fits the SPP exciting angle $\theta_{spp}$) can excite the SPP on a ring-shaped region of gold film [SPP excitation ring in Fig. 1(b)]. Then the

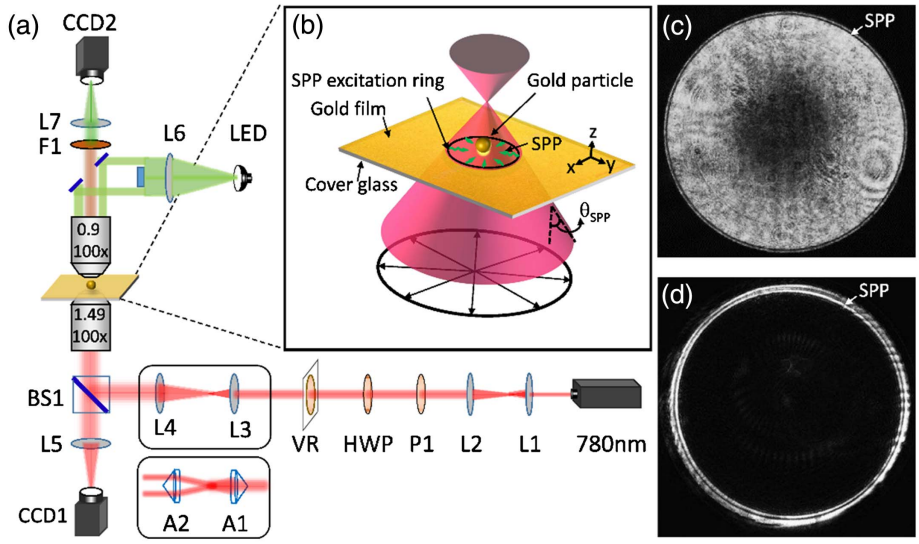


**Fig. 1.** Dynamic plasmonic tweezer system construction and two types of excitation optical beam generation. (a) Technical schematic of the generating RPB and PRPB for the optical tweezer system. The RPB generated by vortex retarder (VR) is also the PRPB generated by changing telescope system (L3, L4) with two axicons (A1, A2). (b) Technical schematic of the SPP excitation process for a focusing RPB. The black arrows indicate the radial polarization directions. (c) The profile of the reflected light obtained at the back focal plane for RPB. (e) The profile of the reflected light obtained at the back focal plane for PRPB.

excited SPP acts as a circular source propagating towards the center [green arrows in Fig. 1(b)] and finally forms a sharp plasmonic focal spot at the center by SPP constructive superposition, which can serve as a highly concentrated source to trap metal particles [4]. Simultaneously, a part of the RPB directly transmits through the gold film and forms a focus above the film, and the other part of the RPB is reflected or absorbed by the gold film.

The profiles of reflected light at the back focal plane can be obtained by CCD1 in Fig. 1(a), and the results are shown in Figs. 1(c) and 1(d) for the RPB and PRPB, respectively. The sharp dark rings in Figs. 1(c) and 1(d) represent the almost zero reflection at the SPP exciting angle [29], verifying that the SPP has been efficiently excited at the ring-shaped position in both cases. Here the diameter of the PRPB is modulated to perfectly match the SPP exciting angle, thus improving the SPP exciting efficiency and eliminating the influence of directly transmitted light.

## 3. RESULTS AND DISCUSSION

To demonstrate that the PRPB is more efficient than the RPB in a plasmonic trap, the finite difference time-domain (FDTD) method is used to calculate the electric field distributions of the SPP at the gold–water interface. As shown in Figs. 2(a)–2(c), the schematics depict three cases: two cases with SPP excitation (RPB and PRPB with high-NA focusing) and the other one without SPP excitation (RPB with lower-NA focusing). The black arrows in the cross sections of all beams indicate the radial polarization directions. The very narrow yellow ring in the beam cross section represents part of the beam fitting the SPP exciting angle [corresponding to the dark ring shown in Figs. 1(c) and 1(d)]; thus, here the diameter of the PRPB is optimized to just cover the yellow ring, as shown in Fig. 2(b). To clearly show the effect of the directly transmitted light, in Fig. 2(c) we consider another case of an RPB focused with a lower NA, whose maximum deflection angle for the incident beam is smaller than the SPP exciting angle; thus, there is no excited SPP field and only the contribution of the direct transmission part of the RPB remains.

Figures 2(d)–2(i) present the distributions of electric field intensity at the gold–water interface and in the $x$-$z$ plane for the three cases. In Figs. 2(d) and 2(g), the electric field distribution of the RPB case is actually a superposition of the excited SPP field and the direct transmission part of the RPB, where the latter is stronger and forms a bright focus at $z = 3$ μm in Fig. 2(g). For the case of PRPB, Figs. 2(e) and 2(h) depict the electric field distributions, where the excited SPP field dominates and the directly transmitted light is efficiently eliminated. Because the SPP exciting angle is constant, the PRPB-excited SPP field distribution [Fig. 2(e)] is similar to that of the RPB [Fig. 2(d)], but the excitation efficiency of the SPP is highly improved. The central peak intensity of the SPP field excited by the PRPB [Fig. 2(e)] is much stronger than in the RPB case [Fig. 2(d)], proving that the SPP exciting efficiency is improved by the PRPB. In Figs. 2(f) and 2(i), the SPP field is not excited and only the direct transmission light forms a strong focus [Fig. 2(i)], which could greatly influence the trapping stiffness. From the comparison of the three cases in Fig. 2, we can find that the directly transmitted light could be the main factor of

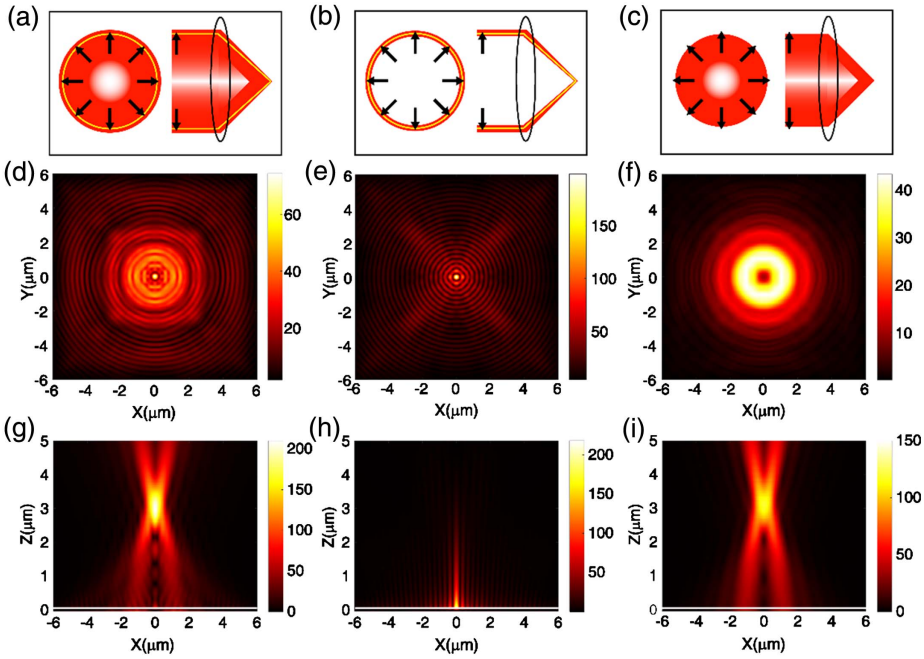


**Fig. 2.** Calculated electric field intensities at the gold–water interface for focused RPB and PRPB. (a), (b), (c) Cross-section distribution and focused state for RPB, PRPB and RPB with no SPP excitation mode. (d), (g) Electric field intensities at the gold–water interface (horizontal $x$-$y$ plane) and in the $x$-$z$ plane for RPB. (e), (h) Electric field intensities at the gold–water interface ($x$-$y$ plane) and in the $x$-$z$ plane for the PRPB. (f), (i) Electric field intensities at the gold–water interface ($x$-$y$ plane) and in the $x$-$z$ plane for the RPB with no SPP excitation mode. The white lines in the bottom of (g), (h), and (i) indicate the gold–water interface.

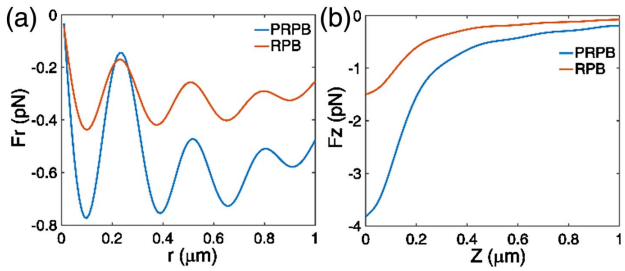


**Fig. 3.** Calculated force distributions at the gold–water interface for the focused RPB and PRPB. (a) Distributing curve of force for gold particles in the radial direction with the RPB and PRPB. (b) Distributing curve of force for gold particles in axial direction with the RPB and PRPB.

instability for trapping particles, and the PRPB is a better choice than RPB in a plasmonic trapping system.

Additionally, the optical forces acting on the particle located in both fields are calculated through the Maxwell stress tensor method [30]. All structures and parameters chosen in the calculation are exactly according to the experimental conditions, i.e., the gold film thickness is set to be 50 nm, the diameter of the particle is 1 μm, and the gap between the particle and the gold film is 10 nm. Figure 3 shows the calculated optical forces, a negative force ($F_r < 0$) along the radial direction shows an attracting effect on particles towards the central optical axis, and conversely the positive force ($F_r > 0$) pushes them away. As compared in Figs. 3(a) and 3(b), the trapping force in the radial direction ($F_r$) is always smaller than that in axial direction ($F_z$) in both the RPB and PRPB cases, demonstrating that the excited SPP field mainly generates a stronger force in the $-z$ direction to drag particles down to the metal surface. In Fig. 3(a), when the particle deviates from the center, $F_r$ is always smaller than 0 and thus forms a potential well to trap particles, and the quasi-periodic variation of $F_r$ originates from the interference fringes of the SPP field [Fig. 2(e)]. In Fig. 3(b), the force $F_z$ reduces as the particle moves away from surface due to the evanescent property of the SPP field in the $z$ direction. The SPP field intensity shows exponential decay along the $z$ direction, and the transverse force decreases but remains similar to that on the surface when the particle moves away. In both results of $F_r$ and $F_z$, the PRPB case always provides larger trapping forces than the RPB, corresponding to the stronger SPP field excited by the PRPB shown in Fig. 2.

Trapping stiffness is an appropriate quantity to illustrate the efficiency of optical tweezers [2]. To verify the numerical studies above, trapping experiments were implemented, and the dynamic processes were recorded for trapping stiffness analysis. Traditionally, a quadrant photodiode (QPD) was usually used to measure the position of trapped particles and analyze the trapping stiffness [2,31], as it can offer precise and high-bandwidth measurements with typical frequencies of several kilohertz (kHz). However, a QPD is not suitable for the plasmonic tweezers here. Due to the high absorption and reflection of incident light by the gold film, only a small part of light can transmit through the film, especially for the PRPB. Therefore, there is not enough scattering light captured by QPD, which could affect the sensitivity of particle localization. Consequently, in the experiment we chose another approach based on a high-speed video camera to measure the particle position and force, which is also widely used [31–34]. Herein, a high-speed CMOS camera (Pointgrey GS3-U3-23S6M-C) was used to capture the dynamic process of the trapped particles with a frame rate of 150 Hz. Image sequences were captured for trapped particles with different diameters and at different power levels, where a region of interest (ROI) was chosen with different resolutions depending on the displacement range of the trapped particles. The plasmonic tweezers control and the video capturing was performed by a custom-made LabVIEW program.

To retrieve the motion data from the image sequences, an image registration technique, phase correlation (PC) [35] of the Fourier transform method, is adopted to achieve sub-pixel motion resolution [33]. Figures 4(a) and 4(d) give the retrieved position distributions of a trapped gold particle in a focused SPP field excited by the RPB and PRPB, respectively. The corresponding sub-pixel displacement versus time is displayed in Figs. 4(b) and 4(e) for both the $x$ and $y$ axes, similar to the performance of a QPD. From the experimental data distributions, we can see the displacement distribution satisfies normal distribution. The full width at half-maximum (FWHM) for RPB displacement is $631 \pm 50$ nm and for PRPB displacement is $311 \pm 10$ nm, clearly showing that the stability for PRPB increases to about twice of that of the RPB.

It is well known that a trapping force exerted on particles can be considered following Hooke's law, where trap force is proportional to the displacement with a stiffness constant $k$. The trap stiffness is determined via $k = 2\pi\gamma f_c$, where $f_c$ is the cutoff frequency obtained from the displacement power spectrum density (PSD) of the trapped particles, and $\gamma$ is the resistance coefficient determined via $\gamma = 6\pi r\eta$, with $r$ and $\eta$ being the radius of the trapped particle and the viscosity coefficient of water ($\eta = 5.465 \times 10^{-5}$) [18], respectively. Based on the motion data, we calculate the displacement PSD of the trapped particles, as shown in Figs. 4(c) and 4(f). The least-squares fitting of a Lorentzian was performed to obtain the cutoff frequency $f_c$ [36]. The whole image processing and power spectrum analysis were performed by a custom-made MATLAB program. We can find that the PSD distribution for the PRPB is less smooth than that of the RPB at nearly the same excited laser power. The fitted cutoff frequencies are $2.75 \pm 0.17$ Hz and $7.20 \pm 0.19$ Hz for the RPB and PRPB, respectively. Thus, the calculated plasmonic trapping stiffnesses are $0.89 \pm 0.005$ pN/μm and $2.33 \pm 0.006$ pN/μm for RPB and PRPB, respectively. The experiment results demonstrate that the PRPB has about 2.6 times enhancement over RPB in plasmonic trapping stiffness; thus, the PRPB is a better choice than RPB in a plasmonic trapping system, agreeing well with the numerical studies above.

Finally, to further demonstrate the trapping ability of the PRPB, we measured the transverse trapping stiffness of the RPB and PRPB under different incident laser powers and particle diameters, as shown in Figs. 5(a) and 5(b), respectively. In Fig. 5(a), the stiffness grows with the increase of incident

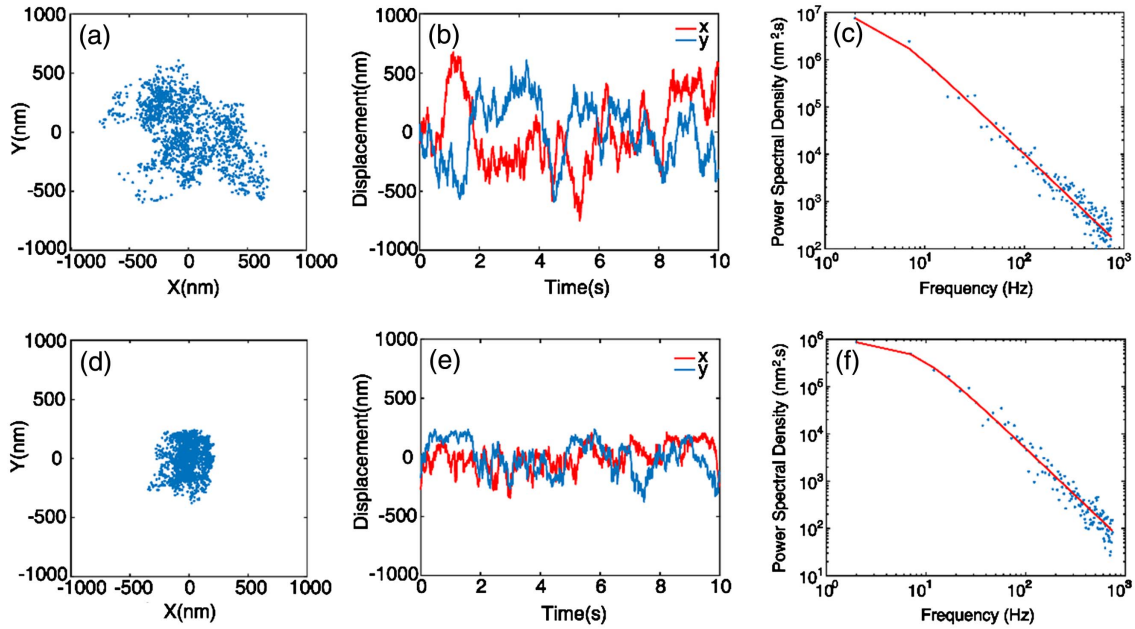


**Fig. 4.** Position tracking and power spectra analysis of the trapped gold particles with a diameter of $1 \pm 0.5$ μm for (a)–(c) RPB and (d)–(f) PRPB. The laser powers at the BFP are about 13.9 mW and 12.4 mW for the RPB and PRPB, respectively. (a) Scattering distribution of the position for the gold particle in RPB. (b) Displacement of the particle versus time for RPB. (c) The power spectra of the particle for RPB fitting with a Lorentzian curve. (d) Scattering distribution of the position for the gold particle in PRPB. (e) Displacement of the particle versus time for PRPB. (f) The power spectra of the particle for PRPB fitting with a Lorentzian curve.

laser power, and the stiffness of the PRPB is also about twice larger compared with that of the RPB at different laser powers. However, it is worth noting that when the laser power is high enough, the trap would become unstable and the trapping stiffness could decrease, because the photothermal effect aggravates the Brownian motion. Additionally, as the laser power increases, the particles are easy to aggregate in the center of the potential well [9,11], which could destroy the optical field and make the particle more unstable. In Fig. 5(b), we can find the trapping stiffness increases as the particle diameter increases for both RPB and PRPB cases, and the stiffness enhancement due to PRPB is also about twice the size with different diameters.

Both theoretical and experimental results demonstrate that a PRPB with a tunable sharp ring can reduce the scattering force on the trapped particle and enhance the plasmonic field as well as trapping stiffness. Consequently, a PRPB is more efficient than an RPB in exciting SPP tweezers.

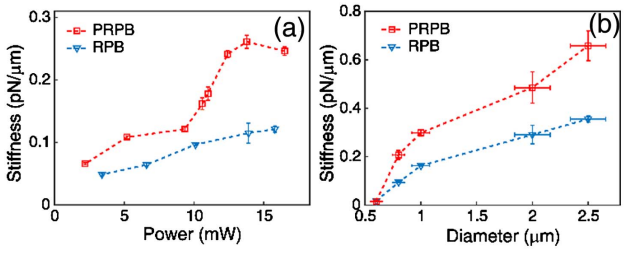


**Fig. 5.** Trapping stiffness as a function of laser power and particle diameter. (a) Transverse trapping stiffness as a function of laser power for 1 μm gold particles trapped by RPB and PRPB. (b) Transverse trapping stiffness as a function of gold particles diameter for laser power at 12.4 mW trapped by RPB and PRPB.

## 4. CONCLUSIONS

In conclusion, through adding an axicon pair in a conventional dynamic SPP optical tweezer system with RPB, we successfully constructed a more efficienct plasmonic tweezers system with PRPB. The ring-shaped PRPB can be tuned such that the power of the beam is mainly concentrated at the SPP exciting angle under a tight focusing configuration, while the direct transmission light through the metallic film was suppressed. We have theoretically and experimentally demonstrated that the PRPB has a higher efficiency in trapping metal particles than RPB, and significantly improves the excitation efficiency of SPP. PRPB has shown high efficiency both on particle trapping and field enhancement, which provides great potential in many applications, such as dynamic SERS measurement and imaging, nanostructure fabrication, and lab-on-a-chip research.

**Funding.** National Natural Science Foundation of China (NSFC) (61427819, 61490712, 91750205, U1701661, 61605117, 11604219); National Key Basic Research Program of China (973) (2015CB352004); National Key Research and Development Program of China (2016YFC0102401); Leading Talents Program of Guangdong Province (00201505); Natural Science Foundation of Guangdong Province (2016A030312010, 2016A030310063, 2017A030313351); Science and Technology Innovation Commission of Shenzhen (KQTD2015071016560101, KQTD2017033011044403, ZDSYS201703031605029, JCYJ2017818144338999);

Excellent Young Teacher Program of Guangdong Province (YQ2014151); China Post-doctoral Science Foundation (2017M612722).

†These authors contributed equally to this work.

## REFERENCES


1. A. Ashkin, "Acceleration and trapping of particles by radiation pressure," Phys. Rev. Lett. **24**, 156–159 (1970).
2. K. C. Neuman and S. M. Block, "Optical trapping," Rev. Sci. Instrum. **75**, 2787–2809 (2004).
3. P. K. Jain, X. H. Huang, I. H. El-Sayed, and M. A. El-Sayed, "Noble metals on the nanoscale: optical and photothermal properties and some applications in imaging, sensing, biology, and medicine," Acc. Chem. Res. **41**, 1578–1586 (2008).
4. K. Svoboda and S. M. Block, "Optical trapping of metallic Rayleigh particles," Opt. Lett. **19**, 930–932 (1994).
5. P. M. Hansen, V. K. Bhatia, N. Harrit, and L. Oddershede, "Expanding the optical trapping range of gold nanoparticles," Nano Lett. **5**, 1937–1942 (2005).
6. R. Quidant and C. Girard, "Surface-plasmon-based optical manipulation," Laser Photon. Rev. **2**, 47–57 (2008).
7. O. M. Marago, P. H. Jones, P. G. Gucciardi, G. Volpe, and A. C. Ferrari, "Optical trapping and manipulation of nanostructures," Nat. Nanotechnol. **8**, 807–819 (2013).
8. T. Shoji and Y. Tsuboi, "Plasmonic optical tweezers toward molecular manipulation: tailoring plasmonic nanostructure, light source, and resonant trapping," J. Phys. Chem. Lett. **5**, 2957–2967 (2014).
9. C. J. Min, Z. Shen, J. F. Shen, Y. Q. Zhang, H. Fang, G. H. Yuan, L. P. Du, S. W. Zhu, T. Lei, and X. C. Yuan, "Focused plasmonic trapping of metallic particles," Nat. Commun. **4**, 2891 (2013).
10. Y. Q. Zhang, J. Wang, J. F. Shen, Z. S. Man, W. Shi, C. J. Min, G. H. Yuan, S. W. Zhu, H. P. Urbach, and X. C. Yuan, "Plasmonic hybridization induced trapping and manipulation of a single Au nanowire on a metallic surface," Nano Lett. **14**, 6430–6436 (2014).
11. P. P. Patra, R. Chikkaraddy, R. P. N. Tripathi, A. Dasgupta, and G. V. P. Kumar, "Plasmofluidic single-molecule surface-enhanced Raman scattering from dynamic assembly of plasmonic nanoparticles," Nat. Commun. **5**, 4357 (2014).
12. L. C. Zhang, X. J. Dou, C. J. Min, Y. Q. Zhang, L. P. Du, Z. W. Xie, J. F. Shen, Y. J. Zeng, and X. C. Yuan, "In-plane trapping and manipulation of ZnO nanowires by a hybrid plasmonic field," Nanoscale **8**, 9756–9763 (2016).
13. L. H. Lin, J. L. Zhang, X. L. Peng, Z. L. Wu, A. C. H. Coughlan, Z. M. Mao, M. A. Bevan, and Y. B. Zheng, "Opto-thermophoretic assembly of colloidal matter," Sci. Adv. **3**, e1700458 (2017).
14. Z. Shen, Z. J. Hu, G. H. Yuan, C. J. Min, H. Fang, and X. C. Yuan, "Visualizing orbital angular momentum of plasmonic vortices," Opt. Lett. **37**, 4627–4629 (2012).
15. M. E. J. Friese, J. Enger, H. Rubinsztein-Dunlop, and N. R. Heckenberg, "Optical angular-momentum transfer to trapped absorbing particles," Phys. Rev. A **54**, 1593–1596 (1996).
16. Y. F. Yuan, Y. N. Lin, B. B. Gu, N. Panwar, S. C. Tjin, J. Song, J. L. Qu, and K. T. Yong, "Optical trapping-assisted SERS platform for chemical and biosensing applications: design perspectives," Coord. Chem. Rev. **339**, 138–152 (2017).
17. Y. Q. Zhang, J. F. Shen, Z. W. Xie, X. J. Dou, C. J. Min, T. Lei, J. Liu, S. W. Zhu, and X. C. Yuan, "Dynamic plasmonic nano-traps for single molecule surface-enhanced Raman scattering," Nanoscale **9**, 10694–10700 (2017).
18. M. Dienerowitz, M. Mazilu, and K. Dholakia, "Optical manipulation of nanoparticles: a review," J. Nanophoton. **2**, 021875 (2008).
19. D. Bhalothia and Y. T. Yang, "Trapping of micro particles in nanoplasmonic optical lattice," J. Visualized Exp. e56151 (2017).
20. K. Wang, E. Schonbrun, P. Steinvurzel, and K. B. Crozier, "Trapping and rotating nanoparticles using a plasmonic nano-tweezer with an integrated heat sink," Nat. Commun. **2**, 469 (2011).
21. A. Yang, L. Du, X. Dou, F. Meng, C. Zhang, C. Min, J. Lin, and X. Yuan, "Sensitive gap-enhanced Raman spectroscopy with a perfect radially polarized beam," Plasmonics **13**, 991–996 (2017).
22. Q. W. Zhan, "Cylindrical vector beams: from mathematical concepts to applications," Adv. Opt. Photon. **1**, 1–57 (2009).
23. K. Kitamura, K. Sakai, and S. Noda, "Sub-wavelength focal spot with long depth of focus generated by radially polarized, narrow-width annular beam," Opt. Express **18**, 4518–4525 (2010).
24. A. S. Ostrovsky, C. Rickenstorff-Parrao, and V. Arrizon, "Generation of the "perfect" optical vortex using a liquid-crystal spatial light modulator," Opt. Lett. **38**, 534–536 (2013).
25. P. Vaity and L. Rusch, "Perfect vortex beam: Fourier transformation of a Bessel beam," Opt. Lett. **40**, 597–600 (2015).
26. M. Lei, Z. Li, S. H. Yan, B. L. Yao, D. Dan, Y. J. Qi, J. Qian, Y. L. Yang, P. Gao, and T. Ye, "Long-distance axial trapping with focused annular laser beams," PLoS ONE **8**, e57984 (2013).
27. Y. C. Liu, Y. G. Ke, J. X. Zhou, Y. Y. Liu, H. L. Luo, S. C. Wen, and D. Y. Fan, "Generation of perfect vortex and vector beams based on Pancharatnam-Berry phase elements," Sci. Rep. **7**, 44096 (2017).
28. M. V. Jabir, N. A. Chaitanya, A. Aadhi, and G. K. Samanta, "Generation of 'perfect' vortex of variable size and its effect in angular spectrum of the down-converted photons," Sci. Rep. **6**, 21877 (2016).
29. L. P. Du, G. H. Yuan, D. Y. Tang, and X. C. Yuan, "Tightly focused radially polarized beam for propagating surface plasmon-assisted gap-mode Raman spectroscopy," Plasmonics **6**, 651–657 (2011).
30. M. Born and E. Wolf, *Principles of Optics* (Cambridge University, 1999).
31. M. Sarshar, W. S. T. Wong, and B. Anvari, "Comparative study of methods to calibrate the stiffness of a single-beam gradient-force optical tweezers over various laser trapping powers," J. Biomed. Opt. **19**, 115001 (2014).
32. G. M. Gibson, J. Leach, S. Keen, A. J. Wright, and M. J. Padgett, "Measuring the accuracy of particle position and force in optical tweezers using high-speed video microscopy," Opt. Express **16**, 14561–14570 (2008).
33. J. P. Staforelli, E. Vera, J. M. Brito, P. Solano, S. Torres, and C. Saavedra, "Superresolution imaging in optical tweezers using high-speed cameras," Opt. Express **18**, 3322–3331 (2010).
34. A. van der Horst and N. R. Forde, "Power spectral analysis for optical trap stiffness calibration from high-speed camera position detection with limited bandwidth," Opt. Express **18**, 7670–7677 (2010).
35. M. Druckmuller, "Phase correlation method for the alignment of total solar eclipse images," Astrophys. J. **706**, 1605–1608 (2009).
36. K. Berg-Sorensen and H. Flyvbjerg, "Power spectrum analysis for optical tweezers," Rev. Sci. Instrum. **75**, 594–612 (2004).